Connecting the molecular scale to the continuum scale for diffusion processes in smectite-rich porous media

IAN C. BOURG* AND GARRISON SPOSITO

Geochemistry Department, Earth Sciences Division, Lawrence Berkeley National Laboratory, Berkeley, CA 94720, USA

*Author to whom correspondence should be addressed (icbourg@lbl.gov; phone: 510-486-7393; fax: 510-643-2940)

Abstract

In this paper, we address the manner in which the continuum-scale diffusive properties of smectite-rich porous media arise from their molecular- and pore-scale features. Our starting point is a successful model of the continuum-scale apparent diffusion coefficient for water tracers and cations which decomposes it as a sum of pore-scale terms describing diffusion in macropore and interlayer "compartments." We then apply molecular dynamics (MD) simulations to determine molecular-scale diffusion coefficients $D_{interlayer}$ of water tracers and representative cations (Na^+, Cs^+, Sr^{2+}) in Na-smectite interlayers. We find that a remarkably simple expression relates $D_{interlayer}$ to the pore-scale parameter $\delta_{nanopore} \leq 1$, a constrictivity factor that accounts for the lower mobility in interlayers as compared to macropores: $\delta_{nanopore} = D_{interlayer}/D_0$, where D_0 is the diffusion coefficient in bulk liquid water. Using this scaling expression, we can accurately predict the apparent diffusion coefficients of tracer H_2O, Na^+, Sr^{2+} and Cs^+ in compacted Na-smectite-rich materials.

Introduction

How do continuum-scale transport properties arise from the molecular- and pore-scale features of porous media? In the present paper, we address this abiding question for the particular case of the "apparent" diffusion coefficient D_a [defined by the continuum-scale relation $N_i \equiv D_{a,i}\, \partial C^*/\partial x_i$, if N_i is the mass flux density of the species of interest along the x_i direction and C^* is its total concentration per volume of porous medium] of water tracers and dissolved solutes in smectite-rich porous media. These diffusion coefficients are widely used in reconstructing the geochemistry of sedimentary formations (1, 2) and in predicting the performance of natural or engineered contaminant barrier systems (3, 4), radioactive waste repositories (5, 6), and CO_2 repositories (7, 8).

We have previously investigated the relationship between D_a and the pore-scale features of water-saturated smectite-rich porous media (9-11), finding that D_a values of water and cations can be modeled rather simply as a sum of two terms describing diffusion in macropore and smectite interlayer nanopore "compartments":

$$D_{a,i}/D_0 = 1/G_i\,(\alpha_{macropore} + \alpha_{nanopore}\delta_{nanopore}) \qquad (1)$$

In Eq. 1, D_0 is the diffusion coefficient of the species of interest in bulk liquid water, G_i is a "geometry factor" that accounts for tortuosity, pore connectivity and pore-size variability (12), $\alpha_{macropore}$ and $\alpha_{nanopore}$ are the mole fractions of the species of interest located in macropores and smectite interlayer nanopores, respectively ($\alpha_{macropore} + \alpha_{nanopore} = 1$ if adsorption on smectite edge surfaces or on non-smectitic minerals is negligible), and $\delta_{nanopore}$ is a "constrictivity factor" that accounts for the lower mobility of species in interlayers as compared to macropores (13). Equation 1 shares a conceptual basis (the treatment of interlayer nanopores as a well-defined compartment of the overall pore space) with models of surface geochemistry (14) and chemo-

mechanical coupling in argillaceous porous media (15, 16). We note in passing that the well-known slower diffusion of water tracers and solutes in nanopores than in bulk liquid water also has been modeled by defining an overall δ value [alternatively called α (17), $\alpha_a g$ (18), or q (19)] for the entire pore space, such that $D_{a,i}/D_0 = \delta/G_i$ (13), whereas Eq. 1 explicitly distinguishes between macropores and nanopores, analogous to the approach recently used by Hirono et al. (20) to interpret ionic diffusion in rocks from the oceanic floor and continental sedimentary formations. Despite its simplicity, Eq. 1 successfully predicts the influence of dry bulk density, smectite content, and ionic strength on the D_a values for water tracers, Na^+, and Sr^{2+} in Na-smectite-rich clay barriers (9-11).

We estimated $\delta_{nanopore}$ for water tracers, Na^+, and Sr^{2+} in Na-smectite-rich porous media using continuum-scale experimental data on diffusion in films of oriented, partially hydrated Na-smectite lamellae (Table 1, last data column). However, we could not evaluate the relation of $\delta_{nanopore}$ to the molecular-scale diffusion coefficient $D_{interlayer}$ in individual smectite interlayer nanopores because of the scatter among available estimates of $D_{interlayer}$. For example, previous molecular dynamics (MD) simulations for water tracers in the two-layer hydrate of Na-montmorillonite have yielded $D_{interlayer}/D_0$ ranging from 0.53 to 0.71 (21-23), while quasielastic neutron scattering (QENS) data led to $D_{interlayer}/D_0 = 0.33$ (24).

In the present study, we carried out new MD simulations of Na-montmorillonite interlayers in stacked lamellae (some of which were doped with trace amounts of Sr^{2+} or Cs^+) using (1) water and solute interatomic potentials known to predict diffusion in bulk liquid water accurately (25-27), (2) the most recent *ab initio* estimates of clay atom partial charges (28), and (3) MD simulation times 10 to 50 times longer than in most previous studies (22, 23, 29, 30). Our simulation results are consistent with the best available neutron diffraction and QENS data on the

structure and dynamics of interlayer water (24, 31). Calculations of $D_{interlayer}$ for tracer H_2O, Na^+, and Sr^{2+} in saturated Na-montmorillonite suggest the very simple scaling relationship: $\delta_{nanopore} = D_{interlayer}/D_0$. Using this relationship, we can predict continuum-scale D_a values of tracer H_2O, Na^+, Sr^{2+}, and Cs^+ in Na-smectite-rich clay barriers.

Molecular Dynamics Simulations

Methods. Molecular dynamics simulations of Na-montmorillonite interlayer nanopores (1-, 2- and 3-layer hydrates) were carried out in the microcanonical (*NVE*) ensemble with the program MOLDY 3.6 (32). Our periodically-replicated simulation cell contained two parallel lamellae of Otay-type montmorillonite, each composed of 18 unit cells (dimensions 30.8928 × 26.9937 Å in the basal plane), and two water-filled interlayers (Fig. 1). Montmorillonite atomic coordinates were fixed based on the pyrophyllite structure of Bickmore et al. (33). Stacked lamellae were shifted by random, fixed lengths in directions parallel to the basal plane to avoid perfect stacking registry. The negative structural charge (1.13 $mol_c\ kg^{-1}$) resulted from 30 isomorphic substitutions of Al^{3+} by Mg^{2+} randomly scattered in the octahedral sheet [average unit cell formula $Si_8(Al_{3.167}Mg_{0.833})O_{20}(OH)_4$] under the constraint that substitutions could not occur in adjacent OH-sharing octahedral sites (34). To simulate the one-, two- and three-layer hydrates, we fixed the basal spacing at 12.5, 15.5 or 18.5 Å (35-39) and the interlayer water content at 5 H_2O per unit cell per water layer.

Our primary interest being diffusion, we used the extended simple point charge (SPC/E) model (40) along with water-solute inter-atomic potentials (25, 41, 42) known to describe diffusion in bulk liquid water accurately (25-27). For montmorillonite, we used the estimates of clay atom partial charges and short-range interaction parameters developed by Cygan et al. (28).

We investigated three interlayer cation compositions. In the "Na-MMT" simulations, we placed 15 Na^+ into each hydrated interlayer, and in the "Na(Cs)-MMT" and "Na(Sr)-MMT" simulations, we doped one Cs^+ or Sr^{2+} into each interlayer after removing Na^+ to preserve charge balance. Each of our nine systems [one-, two- and three-layer hydrates of Na-, Na(Cs)- and Na(Sr)-MMT] was equilibrated at 298 K during 1.6 ns [3.6 ns for Na(Cs)-MMT], then simulations of 10 (Na-MMT), 20 [Na(Sr)-MMT], or 30 ns [Na(Cs)-MMT] were carried out. Our long simulation times allowed us to investigate the dependence of $D_{\text{interlayer}}$ on the molecular time scale τ. We probed $D_{\text{interlayer}}$ on short time scales ($\tau \leq 6$ ps) with the standard Green-Kubo relation (43):

$$D_{\text{interlayer}} = \frac{1}{2}\lim_{\tau\to\infty}\int_0^{\tau}\left\langle \mathbf{v}_{xy}(0)\cdot\mathbf{v}_{xy}(t)\right\rangle dt, \qquad (2)$$

where $\langle \mathbf{v}_{xy}(0)\cdot\mathbf{v}_{xy}(t)\rangle$ is the velocity autocorrelation function in the interlayer (xy) plane, and on longer time scales with the classic Einstein relation for two-dimensional diffusion (43):

$$D_{\text{interlayer}} = \frac{1}{4}\frac{d\left\langle l_{xy}^2\right\rangle}{d\tau} \qquad (3)$$

where $\langle l_{xy}^2\rangle$ is the mean square displacement in the interlayer plane over a time interval τ.

Validation. The only available experimental data on the molecular structure of water in Na-montmorillonite interlayers appear to be the H/D isotopic-difference neutron diffraction results of Pitteloud et al. (31), expressed as the first-order difference total radial distribution function, $G_H(r)$, the relative probability for coherent neutron scattering by all atoms located non-randomly at the distance r from a D atom minus the same relative probability for an H atom (44) in the two-layer hydrate of Na-montmorillonite at 298 K. Following Park and Sposito (44), we calculated $G_H(r)$ from our MD simulation results as the weighted sum of all possible radial

distribution functions for atoms near an interlayer water proton. Within experimental precision, our MD simulation results (Fig. 2) agree with the data of Pitteloud et al. (31).

Molecular-scale diffusion coefficients of water in porous media can be probed using QENS spectroscopy (45, 46). Marry et al. (24) recently reinterpreted QENS data for hydrated Na-hectorite (a dioctahedral smectite with permanent structural charge in the octahedral sheet) by accounting for the distribution of pore orientations and the anisotropy of interlayer water motions and found $D_{interlayer} = 2.8 \pm 0.4$ and $7.7 \pm 1.0 \times 10^{-10}$ m^2 s^{-1} for water in the one- and two-layer hydrates of Na-montmorillonite on the range of time scales probed by their QENS experiments (1-1000 ps in the one-layer hydrate and 1-100 ps in the two-layer hydrate). Over the same range of probe time scales, our MD simulations yielded $D_{interlayer}$ values of 1.2-4.3 and 6.3-9.0 $\times 10^{-10}$ m^2 s^{-1} for the one- and two-layer hydrates, respectively, which are consistent with the experimental $D_{interlayer}$ values reported by Marry et al. (24). [The $D_{interlayer}$ values calculated by Marry et al. (24) are more sensitive to the upper end of the range of time scales probed by their QENS experiments, therefore our MD simulation methodology likely underestimates $D_{interlayer}$ in the one-layer hydrate.]

Results and Discussion

Influence of Probe Time Scale on $D_{interlayer}$. The relation between $D_{interlayer}/D_0$ and log τ is plotted in Fig. 3 for water, Na^+, Sr^{2+} and Cs^+ in the one-, two- and three-layer hydrates of Na-montmorillonite as deduced from MD simulations using Eqs. 2 and 3. Our results suggest the existence of three modes of molecular motion in Na-smectite interlayers: a "rattling" mode characterized by oscillatory behavior in $D_{interlayer}$ at very short times ($\tau < 2$ ps), a "hindered diffusion" mode characterized by a slow decrease in $D_{interlayer}$ at intermediate times, and a true diffusive mode characterized by essentially constant $D_{interlayer}$ at long times ($\tau > 100$ ps). The

"hindered diffusion" mode is unique to nano-confined water tracers or ionic solutes and does not occur in bulk liquid water, where the "rattling" mode gives way to true diffusion after about 2.5 ps (48). Accurate inference of the diffusion coefficients of water tracers or ionic solutes in Na-smectite interlayers requires probe time scales > 100 ps (46, 49), and even greater than 1 ns for cations that form inner-sphere surface complexes (in our study, all cations in the one-layer hydrate and Cs^+ in the two- and three-layer hydrates formed these complexes). The observed τ-dependence of $D_{interlayer}$ for water tracers has been ascribed to molecules diffusing relatively rapidly in regions of the interlayer space that contain no interlayer cations, while diffusing slowly or infrequently between such regions (29, 49). A similar "hindered diffusion" of cations was observed in our simulations, possibly induced by the difficulty they experienced to displace neighboring cations or travel between clusters of cation exchange sites.

Molecular-Scale Significance of $\delta_{nanopore}$. Using our MD simulation results for $<l_{xy}^2>$ at large τ, we calculated $D_{interlayer}/D_0$ for H_2O tracers, Na^+, Sr^{2+} and Cs^+ in the one-, two- and three-layer hydrates of Na-montmorillonite at 298 K (Table 1, first data column). The average values of $D_{interlayer}/D_0$ for each species in the two- and three-layer hydrates (Table 1, second data column) are remarkably similar to our previous estimates of the values of the pore-scale parameter $\delta_{nanopore}$ under conditions wherein Na-montmorillonite forms these two hydrates (Table 1, third data column). This striking similarity suggests that a simple scaling relationship exists between $\delta_{nanopore}$ and the molecular-scale interlayer diffusion coefficient $D_{interlayer}$:

$$\delta_{nanopore} = D_{interlayer}/D_0 \qquad (4)$$

Equation 4 implies that processes occurring at scales intermediate between the molecular and the continuum do not strongly affect $\delta_{nanopore}$ for water tracers and cations. It is equivalent to expressing $D_{a,i}$ in Eq. 1 as the weighted average of bulk and interlayer molecular diffusion

coefficients, with the weightings given by $\alpha_{macropore}/G_i$ and $\alpha_{nanopore}/G_i$, respectively. We note in passing that the well-known interpretation of diffusion coefficients in terms of the timescale on which a species diffuses a distance equal to its diameter (43) leads to a molecular interpretation of the constrictivity factor $\delta_{nanopore}$ in Eq. 4 as the ratio of this diffusion timescale in bulk liquid water to that in a nanopore.

Bridging the Molecular and Continuum Scales. Using Eq. 4 and our MD simulation estimates of $D_{interlayer}$, we now can reinterpret our previous pore-scale modeling of D_a for water tracers, sodium, and strontium in compacted water-saturated Na-montmorillonite and Na-bentonite (smectite-rich) clay barriers (9-11) and predict the D_a value of cesium using experimental D_a/D_0 values at 298 K for compacted clay barriers compiled by Bourg (50) and Bourg et al. (9-11). Experimental results for the mean principal value of the $\mathbf{D_a}$ tensor for water tracers as a function of partial montmorillonite dry density $\rho_{b,mont}$ (the mass of montmorillonite per volume of montmorillonite and pore space) are shown in Fig. 4; those for $D_{a,i}$ of Na^+ at $\rho_{b,mont}$ = 0.98 kg dm^{-3} as function of ionic strength (I), normalized to $D_{a,i}$ at $I = 0$, are shown in Fig. 5, and those for $D_{a,i}/D_0$ of Na^+, Sr^{2+} and Cs^+ in Na-bentonite hydrated with pure water or low-ionic-strength solutions, normalized to $D_{a,i}/D_0$ for H_2O, are shown as a function of $\rho_{b,mont}$ in Fig. 6.

For the water diffusion data in Fig. 4, Eq. 1 yields (9):

$$D_a/D_0 = 1/G\ (\alpha_{macropore,water} + \alpha_{nanopore,water}\delta_{nanopore,water}) \quad (5)$$

where D_a is the mean principal value of the apparent diffusion coefficient tensor of water tracers, $G = 4.0 \pm 1.6$ is the "mean principal" geometric factor as estimated by Bourg et al. (9), and $\alpha_{nanopore,water}$ is approximated as the volume fraction of interlayer nanopores (9). For the Na^+ diffusion data in Fig. 5, Eq. 1 yields (11):

$$(D_{a,i})_I/(D_{a,i})_{I=0} = (\alpha_{macropore,Na,I} + \alpha_{nanopore,Na,I}\delta_{nanopore,Na})/\delta_{nanopore,Na} \quad (6)$$

because all Na^+ are located in the interlayer at $I = 0$. Mole fractions $\alpha_{macropore,Na,I}$ and $\alpha_{nanopore,Na,I}$ are estimated from charge-balance considerations (11). Finally, for the ratio of cation and water diffusion coefficients in Fig. 6, Eq. 1 yields (10):

$$(D_{a,i}/D_0)_{cation}/(D_{a,i}/D_0)_{water} = \delta_{nanopore,cation}/(\alpha_{macropore,water} + \alpha_{nanopore,water}\delta_{nanopore,water}). \quad (7)$$

The constrictivity factors $\delta_{nanopore}$ used in Eqs. 5-7 were calculated with Eq. 4 using our MD simulation estimates of $D_{interlayer}$ (Table 1, first data column). At $\rho_{b,mont}$ values where X-ray diffraction (XRD) data (39) show only the three-layer hydrate ($0.98 \le \rho_{b,mont} \le 1.27$ kg dm^{-3}) or the two-layer hydrate ($1.57 \le \rho_{b,mont} \le 1.76$ kg dm^{-3}) exists, we used the corresponding MD simulation estimates of $D_{interlayer}$. At $1.27 \le \rho_{b,mont} \le 1.57$ kg dm^{-3}, where XRD data indicate the simultaneous presence of both hydrates, we modeled $D_{interlayer}$ as a weighted average of our MD simulation estimates of $D_{interlayer}$ in the two hydrates, with the weighting factor being the volume fraction of interlayer water located in each hydrate as estimated by Bourg et al. (9). At $\rho_{b,mont} \le$ 0.98 kg dm^{-3}, where XRD data do not reveal the existence of interlayer nanopores and Eq. 1 is not strictly valid, we used our MD simulation estimates of $D_{interlayer}$ in the three-layer hydrate. Equations 5-7 have no fitting parameters except the mean principal geometric factor G. The good agreement between our model predictions and experimental data (Figs. 4-6) indicates that continuum-scale D_a values for water tracers and cations in smectite-rich clay barriers under compaction are consistent, within experimental precision, with our long-time MD simulations of diffusion in nanopores.

Sensitivity of $D_{interlayer}$ to Simulation Parameters. Although our MD simulations used water-water and water-solute interaction potentials known to describe accurately the structure, diffusion coefficient, and static dielectric constant of bulk liquid water (25, 65, 66) as well as the diffusion coefficients and solvation structures of cations in bulk liquid water (26, 27), the

applicability of these potentials to nano-confined water has not been evaluated systematically. However, the fact that water models different from ours (44) also predict the structure of interlayer water within experimental precision (Fig. 2) suggests that confinement in interlayer nanopores does not require revision of our water-water potentials.

Previous smectite interlayer simulations have yielded roughly two-times-larger $D_{interlayer}$ values for tracer H_2O (21-23) and 10 to 20 times larger $D_{interlayer}$ values for Cs^+ in the two-layer hydrate (22, 23). These previous estimates of $D_{interlayer}$ would yield poor fits to the experimental data in Figs. 4-6 if Eq. 4 were used to estimate $\delta_{nanopore}$. A key parameter that may lead to an explanation of the faster diffusion of water and ions found in previous simulation studies is the partial charge of O atoms on the siloxane surface (q_O), which is directly in contact with interlayer water. Most previous MD and MC simulations of water in smectite interlayers (22, 23, 44, 67-71) have followed Skipper et al. (72) in assigning q_O = -0.8 e to the siloxane surface O on the basis of semi-empirical estimates of the partial charge of surface O atoms in Si-O-Si clusters [-0.6 to -0.8 e (73)] and small montmorillonite clusters [-0.93 e (74)]. In our simulations, we used the recent *ab initio* estimate, q_O = -1.05 e by Cygan et al. (28). The resulting greater negative charge of the siloxane surface in our simulations evidently enhances the affinity of this surface for both water molecules and cations, and especially for cations such as Cs^+ that predominantly form inner-sphere surface complexes.

Acknowledgments

The research reported in this paper was supported by the Director, Office of Energy Research, Office of Basic Energy Sciences, of the U.S. Department of Energy under Contract No. DE-AC02-05CH11231. This research used resources of the National Energy Research Scientific

Computing Center, which is supported by the Office of Science of the U.S. Department of Energy under contract No. DE-AC02-05CH11231.

References

(1) Degueldre, C.; Scholtis, A.; Laube, A.; Turrero, M. J.; Thomas, B. Study of the pore water chemistry through an argillaceous formation: a paleohydrochemical approach. *Appl. Geochem.* **2003**, *18*, 55-73.

(2) Gimmi, T.; Waber, H. N.; Gautschi, A.; Rübel, A. Stable water isotopes in pore water of Jurassic argillaceous rocks as tracers for solute transport over large spatial and temporal scales. *Water Resour. Res.* **2007**, *43*, W04410.

(3) Rowe, R. K. Long-term performance of contaminant barrier systems. *Géotechnique* **2005**, *55*, 631-678.

(4) Jo, H. Y.; Benson, C. H.; Edil, T. B. Rate-limited cation exchange in thin bentonitic barrier layers. *Can Geotech. J.* **2006**, *43*, 370-391.

(5) Gaucher, E. C.; Blanc, P.; Matray, J.-M.; Michau, N. Modeling diffusion of an alkaline plume in a clay barrier. *Appl. Geochem.* **2004**, *19*, 1505-1515.

(6) Montes-H, G.; Marty, N.; Fritz, B.; Clement, A.; Michau, N. Modelling of long-term diffusion-reaction in a bentonite barrier for radioactive waste confinement. *Appl. Clay Sci.* **2005**, *30*, 181-198.

(7) Ketzer, J. M.; Carpentier, B.; Le Gallo, Y.; Le Thiez, P. Geological sequestration of CO_2 in mature hydrocarbon fields. Basin and reservoir numerical modelling of the Forties Field, North Sea. *Oil & Gas Sci. Technol. – Rev. IFP* **2005**, *60*, 259-273.

(8) Gherardi, F.; Xu, T.; Pruess, K. Numerical modeling of self-limiting and self-enhancing caprock alteration induced by CO_2 storage in a depleted gas reservoir. *Chem. Geol.* **2007**, *244*, 103-129.

(9) Bourg, I. C.; Sposito, G.; Bourg, A. C. M. Tracer diffusion in compacted, water-saturated bentonite. *Clays Clay Miner.* **2006**, *54*, 363-374.

(10) Bourg, I. C.; Sposito, G.; Bourg, A. C. M. Modeling cation diffusion in compacted water-saturated sodium bentonite at low ionic strength. *Environ. Sci. Technol.* **2007**, *41*, 8118-8122.

(11) Bourg, I. C.; Sposito, G.; Bourg, A. C. M. Modeling the diffusion of Na^+ in compacted water-saturated Na-bentonite as a function of pore water ionic strength. *Appl. Geochem.* **2008**, *23*, 3635-3641.

(12) Dykhuizen, R. C.; Casey, W. H. An analysis of solute diffusion in rocks. *Geochim. Cosmochim. Acta* **1989**, *53*, 2797-2805.

(13) Grathwohl, P. *Diffusion in Natural Porous Media: Contaminant Transport, Sorption/Desorption and Dissolution Kinetics*; Kluwer Academic Publishing: Boston, 1998.

(14) Wersin, P.; Curti, E.; Appelo, C. A. J. Modelling bentonite-water interactions at high solid/liquid ratios: swelling and diffuse double layer effects. *Appl. Clay Sci.* **2004**, *26*, 249-257.

(15) Gajo, A.; Loret, B. The mechanics of active clays circulated by salts, acids and bases. *J. Mech. Phys. Solids* **2007**, *55*, 1762-1801.

(16) Murad, M. A.; Moyne, C. A dual-porosity model for ionic solute transport in expansive clays. *Comput. Geosci.* **2008**, *12*, 47-82.

(17) Li, Y.-H.; Gregory, S. Diffusion of ions in sea water and in deep-sea sediments. *Geochim. Cosmochim. Acta* **1974**, *38*, 703-714.

(18) van Schaik, J. C.; Kemper, W. D.; Olsen, S. R. Contribution of adsorbed cations to diffusion in clay-water systems. *Soil Sci. Soc. Am. Proc.* **1966**, *30*, 17-22.

(19) González Sánchez, F.; Gimmi, T.; Jurányi, F.; Van Loon, L.; Diamond, L. W. Linking the diffusion of water in compacted clays at two different time scales: Tracer through-diffusion and quasielastic neutron scattering. *Environ. Sci. Technol.* **2009**, *43*, 3487-3493.

(20) Hirono, T.; Nakashima, S.; Spiers, C. J. Measurements of ionic diffusivity in various rock samples: Low diffusivity through nanoscale pores. *Int. J. Rock Mech. Mining Sci.* **2008**, *45*, 450-459.

(21) Chang, F.-R. C.; Skipper, N. T.; Sposito, G. Computer simulation of interlayer molecular structure in sodium montmorillonite hydrates. *Langmuir* **1995**, *11*, 2734-2741.

(22) Marry, V.; Turq, P. Microscopic simulations of interlayer structure and dynamics in bihydrated heteroionic montmorillonites. *J. Phys. Chem. B* **2003**, *107*, 1832-1839.

(23) Kosakowski, G.; Churakov, S. V.; Thoenen, T. Diffusion of Na and Cs in montmorillonite. *Clays Clay Miner.* **2008**, *56*, 190-206.

(24) Marry, V.; Malikova, N.; Cadène, A.; Dubois, E.; Durand-Vidal, S.; Turq, P.; Breu, J.; Longeville, S.; Zanotti, J.-M. Water diffusion in a synthetic hectorite by neutron scattering—beyond the isotropic translational model. *J. Phys.: Condens. Matter* **2008**, *20*, 104205.

(25) Smith, D. E.; Dang, L. X. Computer simulations of NaCl association in polarizable water. *J. Chem. Phys.* **1994**, *100*, 3757-3766.

(26) Koneshan, S.; Rasaiah, J. C.; Lynden-Bell, R. M.; Lee, S.H. Solvent structure, dynamics, and ion mobility in aqueous solutions at 25 °C. *J. Phys. Chem. B* **1998**, *102*, 4193-4204.

(27) Bourg, I. C.; Richter, F. M.; Christensen, J. N.; Sposito, G. Isotopic mass-dependence of metal cation diffusion coefficients in liquid water. *Geochim. Cosmochim. Acta* **2010**, in press.

(28) Cygan, R. T.; Liang, J.-J.; Kalinichev, A. G. Molecular models of hydroxide, oxyhydroxide, and clay phases and the development of a general force field. *J. Phys. Chem. B* **2004**, *108*, 1255-1266.

(29) Sutton, R.; Sposito, G. Molecular simulation of interlayer structure and dynamics in 12.4 Å Cs-smectite hydrates. *J. Colloid Interface Sci.* **2001**, *237*, 174-184.

(30) Malikova, N.; Cadène, A.; Marry, V.; Dubois, E.; Turq, P. Diffusion of water in clays on the microscopic scale: Modeling and experiment. *J. Phys. Chem. B* **2006**, *110*, 3206-3214.

(31) Pitteloud, C.; Powell, D. H.; Soper, A. K.; Benmore, C. J. The structure of interlayer water in Wyoming montmorillonite studied by neutron diffraction with isotopic substitution. *Physica B* **2000**, *276-278*, 236-237.

(32) Refson, K. Moldy: A portable molecular dynamics simulation program for serial and parallel computers. *Comput. Phys. Commun.* **2000**, *126*, 310-329.

(33) Bickmore, B. R.; Rosso, K. M.; Nagy, K. L.; Cygan, R. T.; Tadanier, C. J. Ab initio determination of edge surface structures for dioctahedral 2:1 phyllosilicates: Implications for acid-base reactivity. *Clays Clay Miner.* **2003**, *51*, 359-371.

(34) Sainz-Díaz, C. I.; Palin, E. J.; Dove, M. T.; Hernández-Laguna, A. Monte Carlo simulations of ordering of Al, Fe, and Mg cations in the octahedral sheet of smectites and illites. *Amer. Mineral.* **2003**, *88*, 1033-1045.

(35) Norrish, K.; Quirk, J. P. Crystalline swelling of montmorillonite – use of electrolytes to control swelling. *Nature* **1954**, *173*, 255-256.

(36) Calvet, R. Hydratation de la montmorillonite et diffusion des cations compensateurs. *Ann. Agron.* **1973**, *24*, 77-217.

(37) Fu, M. H.; Zhang, Z. Z.; Low, P. F. Changes in the properties of a montmorillonite-water system during the adsorption and desorption of water: Hysteresis. *Clays Clay Miner.* **1990**, *38*, 485-492.

(38) Cases, J. M.; Bérend, I.; Besson, G.; François, M.; Uriot, J. P.; Thomas, F.; Poirier, J. E. Mechanism of adsorption and desorption of water vapor by homoionic montmorillonite. 1. The sodium-exchanged form. *Langmuir* **1992**, *8*, 2730-2739.

(39) Kozaki, T.; Inada, K.; Sato, S.; Ohashi, H. Diffusion mechanism of chloride ions in sodium montmorillonite. *J. Contam. Hydrol.* **2001**, *47*, 159-170.

(40) Berendsen, H. J. C.; Grigera, J. R.; Straatsma, T. P. The missing term in effective pair potentials. *J. Phys. Chem.* **1987**, *91*, 6269-6271.

(41) Åqvist, J. Ion-water interaction potentials derived from free energy perturbation simulations. *J. Phys. Chem.* **1990**, *94*, 8021-8024.

(42) Dang, L. X. Mechanism and thermodynamics of ion selectivity in aqueous solutions of 18-crown-6 ether: A molecular dynamics study. *J. Am. Chem. Soc.* **1995**, *117*, 6954-6960.

(43) Frenkel, D.; Smit, B. *Understanding Molecular Simulation*, 2nd ed.; Academic Press: San Diego, 2002.

(44) Park, S.-H.; Sposito, G. Monte Carlo simulation of total radial distribution functions for interlayer water in Li-, Na-, and K-montmorillonite hydrates. *J. Phys. Chem. B* **2000**, *104*, 4642-4648.

(45) Sposito, G. Theory of quasielastic neutron scattering by water in heterogeneous systems. *Mol. Phys.* **1982**, *47*, 1377-1389.

(46) Michot, L. J.; Delville, A.; Humbert, B.; Plazanet, M.; Levitz, P. Diffusion of water in a synthetic clay with tetrahedral charges by combined neutron time-of-flight measurements and molecular dynamics simulations. *J. Phys. Chem. C* **2007**, *111*, 9818-9831.

(47) Mills, R. Self-diffusion in normal and heavy water in the range 1-45°. *J. Phys. Chem.* **1973**, *77*, 685-688.

(48) Bourg, I. C.; Sposito, G. Molecular dynamics simulations of kinetic isotope fractionation during the diffusion of ionic species in liquid water. *Geochim. Cosmochim. Acta* **2007**, *71*, 5583-5589.

(49) Greathouse, J. A.; Refson, K.; Sposito, G. Molecular dynamics simulation of water mobility in magnesium-smectite hydrates. *J. Am. Chem. Soc.* **2000**, *122*, 11459-11464.

(50) Bourg, I. C. Tracer diffusion of water and inorganic ions in compacted saturated sodium bentonite. Ph.D. Thesis, University of California, Berkeley, 2004.

(51) Nakashima, Y. Nuclear magnetic resonance properties of water-rich gels of Kunigel-V1 bentonite. *J. Nuclear Sci. Technol.* **2004**, *41*, 981-992.

(52) Nakashima, Y. Pulsed field gradient proton NMR study of the self-diffusion of H_2O in montmorillonite gel: Effects of temperature and water fraction. *Amer. Mineral.* **2001**, *86*, 132-138.

(53) Sato, H.; Suzuki, S. Fundamental study on the effect of an orientation of clay particles on diffusion pathway in compacted bentonite. *Appl. Clay Sci.* **2003**, *23*, 51-60.

(54) Suzuki, S.; Sato, H.; Ishidera, T.; Fujii, N. Study on anisotropy of effective diffusion coefficient and activation energy for deuterated water in compacted sodium bentonite. *J. Contam. Hydrol.* **2004**, *68*, 23-37.

(55) Kozaki, T.; Liu, J.; Sato, S. Diffusion mechanism of sodium ions in compacted montmorillonite under different NaCl concentration. *Phys. Chem. Earth* **2008**, *33*, 957-961.

(56) Kozaki, T.; Fujishima, A.; Sato, S.; Ohashi, H. Self-diffusion of sodium ions in compacted sodium montmorillonite. *Nucl. Technol.* **1998**, *121*, 63-69.

(57) Kozaki, T.; Fujishima, A.; Saito, N.; Sato, S.; Ohashi, H. Effects of dry density and exchangeable cations on the diffusion process of sodium ions in compacted montmorillonite. *Eng. Geol.* **2005**, *81*, 246-254.

(58) Liu, J.; Yamada, H.; Kozaki, T.; Sato, S.; Ohashi, H. Effect of silica sand on activation energy for diffusion of sodium ions in montmorillonite and silica sand mixture. *J. Contam. Hydrol.* **2003**, *61*, 85-93.

(59) Kozaki, T.; Sato, H.; Fujishima, A.; Saito, N.; Sato, S.; Ohashi, H. Effect of dry density on activation energy for diffusion of strontium in compacted sodium montmorillonite. *Mat. Res. Soc. Symp. Proc.* **1997**, *465*, 893-900.

(60) Liu, J.; Kozaki, T.; Horiuchi, Y.; Sato, S. Microstructure of montmorillonite/silica sand mixture and its effects on the diffusion of strontium ions. *Appl. Clay Sci.* **2003**, *23*, 89-95.

(61) Sato, H.; Ashida, T.; Kohara, Y.; Yui, M.; Sasaki, N. Effect of dry density on diffusion of some radionuclides in compacted sodium bentonite. *J. Nuclear Sci. Technol.* **1992**, *29*, 873-882.

(62) Kozaki, T.; Sato, H.; Fujishima, A.; Sato, S.; Ohashi, H. Activation energy for diffusion of cesium in compacted sodium montmorillonite. *J. Nuclear Sci. Technol.* **1996**, *33*, 522-524.

(63) Kozaki, T.; Sato, H.; Sato, S.; Ohashi, H. Diffusion mechanism of cesium ions in compacted montmorillonite. *Eng. Geol.* **1999**, *54*, 223-230.

(64) Kozaki, T.; Sato, Y.; Nakajima, M.; Kato, H.; Sato, S.; Ohashi, H. Effect of particle size on the diffusion behavior of some radionuclides in compacted bentonite. *J. Nuclear Mater.* **1999**, *270*, 265-272.

(65) Wasserman, E.; Wood, B.; Brodholt, J. The static dielectric constant of water at pressures up to 20 kbar and temperatures to 1273 K: Experiment, simulations, and empirical equations. *Geochim. Cosmochim. Acta* **1995**, *59*, 1-6.

(66) Hura, G.; Russo, D.; Glaeser, R. M.; Head-Gordon, T.; Krack, M.; Parrinello, M. Water structure as a function of temperature from X-ray scattering experiments and ab initio molecular dynamics. *Phys. Chem. Chem. Phys.* **2003**, *5*, 1981-1991.

(67) Whitley, H. D.; Smith D. E. Free energy, energy, and entropy of swelling in Cs-, Na-, and Sr-montmorillonite clays. *J. Chem. Phys.* **2004**, *120*, 5387-5395.

(68) Meleshyn, A.; Bunnenberg, C. Swelling of Na/Mg-montmorillonites and hydration of interlayer cations: A Monte Carlo study. *J. Chem. Phys.* **2005**, *123*, 074706.

(69) Skipper, N. T.; Lock, P. A.; Titiloye, J. O.; Swenson, J.; Mirza, Z. A.; Howells, W. S.; Fernandez-Alonso, F. The structure and dynamics of 2-dimensional fluids in swelling clays. *Chem. Geol.* **2006**, *230*, 182-196.

(70) Tambach, T. J.; Bolhuis, P. G.; Hensen, E. J. M.; Smit, B. Hysteresis in clay swelling induced by hydrogen bonding: Accurate prediction of swelling states. *Langmuir* **2006**, *22*, 1223-1234.

(71) Rotenberg, B.; Marry, V.; Vuilleumier, R.; Malikova, N.; Simon, C.; Turq, P. Water and ions in clays: Unraveling the interlayer/micropore exchange using molecular dynamics. *Geochim. Cosmochim. Acta* **2007**, *71*, 5089-5101.

(72) Skipper, N. T.; Chang, F.-R. C.; Sposito, G. Monte Carlo simulation of interlayer molecular structure in swelling clay minerals. 1. Methodology. *Clays Clay Miner.* **1995**, *43*, 285-293.

(73) Hass, E. C.; Mezey, P. G.; Plath, P. J. A non-empirical molecular orbital study on Lowenstein's rule and zeolite composition. *J. Mol. Struc.* **1981**, *76*, 389-399.

(74) Delville, A. Structure of liquids at a solid interface: An application to the swelling of clay by water. *Langmuir* **1992**, *8*, 1796-1805.

Table 1. Molecular dynamics simulation estimates of the long time value of $D_{interlayer}/D_0$ in the one-, two- and three-layer hydrates (one, two or three statistical monolayers of water in each smectite interlayer; first data column) and the average value of $D_{interlayer}/D_0$ in the two- and three-layer hydrates (second data column), compared with previous estimates of the continuum-scale model parameter $\delta_{nanopore}$ in conditions where Na-smectites form two- or three-layer hydrates (last data column).

		$D_{interlayer}/D_0$ [a] (MD, this study)	$D_{interlayer}/D_0$ [b] (MD, average for the 2- & 3-layer hydrates)	$\delta_{nanopore}$ [Bourg et al. (9, 10)]
H_2O	1-layer	0.054 ± 0.009		
	2-layer	0.271 ± 0.009	0.35 ± 0.17	0.30 ± 0.05
	3-layer	0.438 ± 0.028		
Na^+	1-layer	0.010 ± 0.005		
	2-layer	0.172 ± 0.023	0.24 ± 0.14	0.32 ± 0.06
	3-layer	0.312 ± 0.032		
Sr^{2+}	1-layer	0.0000 ± 0.0001		
	2-layer	0.093 ± 0.055	0.13 ± 0.07	0.080 ± 0.022
	3-layer	0.167 ± 0.099		
Cs^+	1-layer	0.009 ± 0.005		
	2-layer	0.049 ± 0.041	0.06 ± 0.03	
	3-layer	0.077 ± 0.064		

[a] Calculated with Eq. 3 by linear regression of the slope of $<l_{xy}^2>$ vs. τ for τ = 200-245 ps (H_2O, Na^+), τ = 400-490 ps (Na^+ in the 1-layer hydrate), τ = 1-2 ns (Sr^{2+}), or τ = 1-4 ns (Cs^+). For H_2O and Na^+, confidence intervals were estimated from $D_{interlayer}/D_0$ values obtained for twenty 0.5 ns blocks of each 10 ns simulation (ten 1 ns blocks for Na^+ in the 1-layer hydrate). For Cs^+ and Sr^{2+} confidence intervals were estimated from $D_{interlayer}/D_0$ values obtained for each ion in the x and y directions, assuming that $D_{interlayer}/D_0$ values in the 2- and 3-layer hydrates have similar coefficients of variation.

[b] Confidence intervals were calculated as $2S/\sqrt{2}$, where S is the standard deviation calculated from $D_{interlayer}/D_0$ in the 2- and 3-layer hydrates.

List of Figures

Fig. 1. Snapshot of our MD simulation cell for the two-layer hydrate of Na-montmorillonite, with Na (blue), water O (red) and water H (white) atoms in the interlayer and Si (yellow), Al (green), Mg (blue), O (red) and H (white) atoms in the clay mineral structure.

Fig. 2. The first-order difference total radial distribution function G_H (barn sr^{-1}) in the two-layer hydrate of Na-montmorillonite, plotted as a function of interatomic distance r (Å) [dotted blue line: experimental results (31); thin red line: previous MC simulation results (44); thick black line: our MD simulation results]. The peak at $r = 3.2$ Å (resulting from second-nearest-neighbor water and clay O atoms) characterizes the medium-range hydrogen-bonding structure of interlayer water. Experimental peaks at $r < 2.7$ Å are likely artifacts (44).

Fig. 3. Molecular dynamics simulation estimates of $D_{interlayer}/D_0$ vs. log τ at 298 K for H_2O, Na^+, Sr^{2+} and Cs^+ in the one-, two- and three-layer hydrates of Na-montmorillonite at 298 K calculated with Eq. 2 ($\tau \leq 6$ ps) or Eq. 3 ($\tau \geq 10$ ps) using $D_0 = 2.3$, 1.33, 0.794, and 2.07×10^{-9} m^2 s^{-1} for H_2O (47), Na^+, Sr^{2+} and Cs^+ (17).

Fig. 4. Semilog plot of the mean principal value of the apparent diffusion coefficient tensor $\mathbf{D_a}$ of water tracers, normalized to D_0, vs. partial montmorillonite dry density $\rho_{b,mont}$ (9). Model predictions were obtained with Eqs. 4-5.

Fig. 5. The $D_{a,i}$ values for Na^+ diffusing in Na-montmorillonite at ionic strength I and $\rho_{b,mont}$ = 0.98 kg dm^{-3}, normalized to $D_{a,i}$ at I = 0 and plotted as a function of I (11). Model predictions were obtained with Eqs. 4 and 6.

Fig. 6. Semilog plots of $D_{a,i}/D_0$ values for Na^+, Sr^{2+} (10) and Cs^+ (49), normalized to $D_{a,i}/D_0$ for water tracers, vs. $\rho_{b,mont}$ for Na-bentonite hydrated with pure water or low-ionic-strength solutions. Model predictions were obtained with Eqs. 4 and 7.

Figure 1.

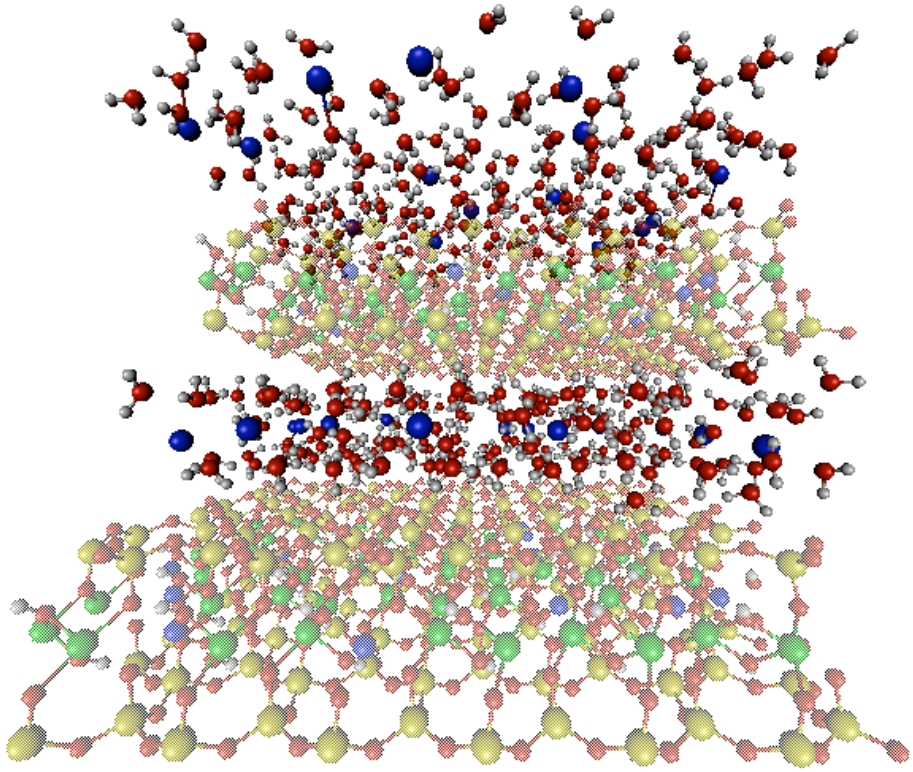

Figure 2.

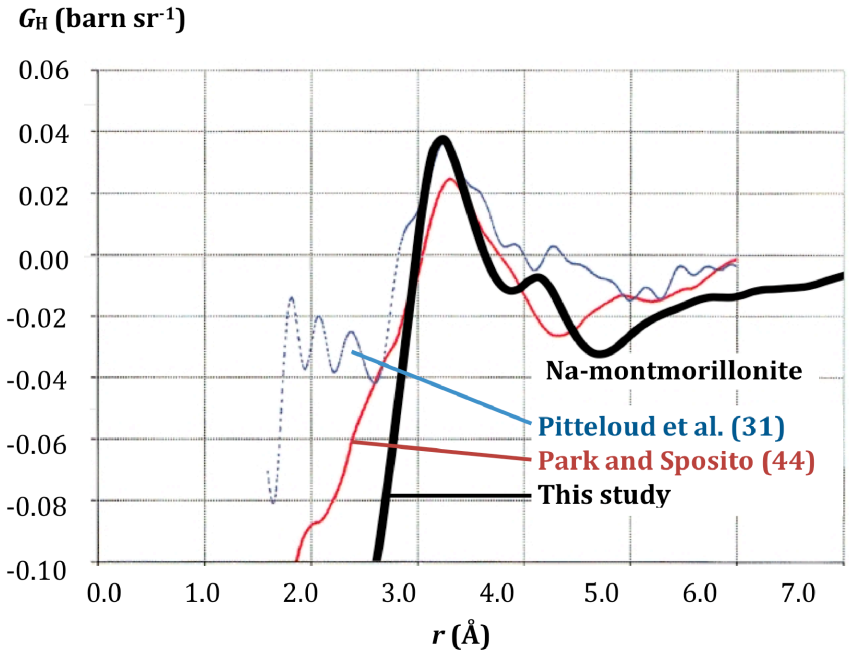
G_H (barn sr^{-1})
0.06
0.04
0.02
0.00
-0.02
-0.04
-0.06
-0.08
-0.10
0.0
1.0
2.0
3.0
4.0
5.0
6.0
7.0
r (Å)
Na-montmorillonite
Pitteloud et al. (31)
Park and Sposito (44)
This study

Figure 3.

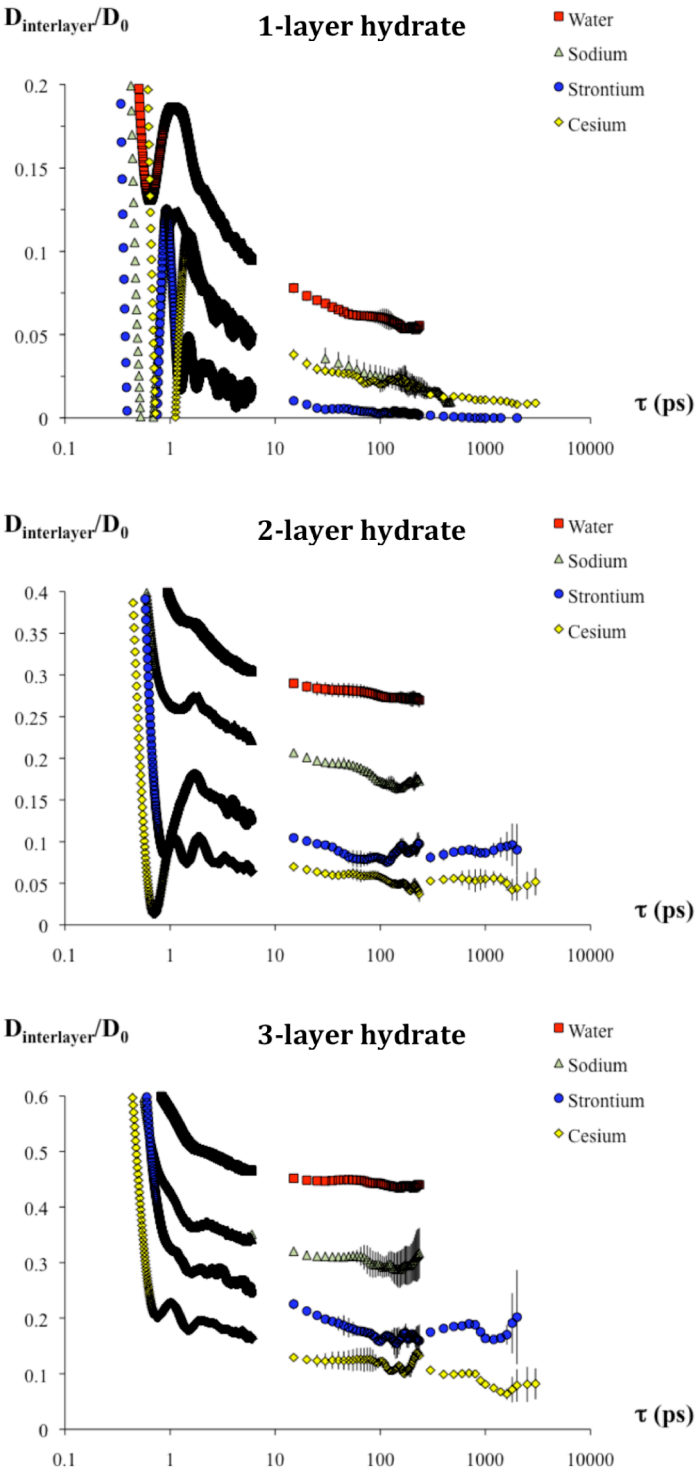
$D_{interlayer}/D_0$
1-layer hydrate
Water
Sodium
Strontium
Cesium
0.2
0.15
0.1
0.05
0
0.1
1
10
100
1000
10000
τ (ps)
$D_{interlayer}/D_0$
2-layer hydrate
Water
Sodium
Strontium
Cesium
0.4
0.35
0.3
0.25
0.2
0.15
0.1
0.05
0
0.1
1
10
100
1000
10000
τ (ps)
$D_{interlayer}/D_0$
3-layer hydrate
Water
Sodium
Strontium
Cesium
0.6
0.5
0.4
0.3
0.2
0.1
0
0.1
1
10
100
1000
10000
τ (ps)

Figure 4.

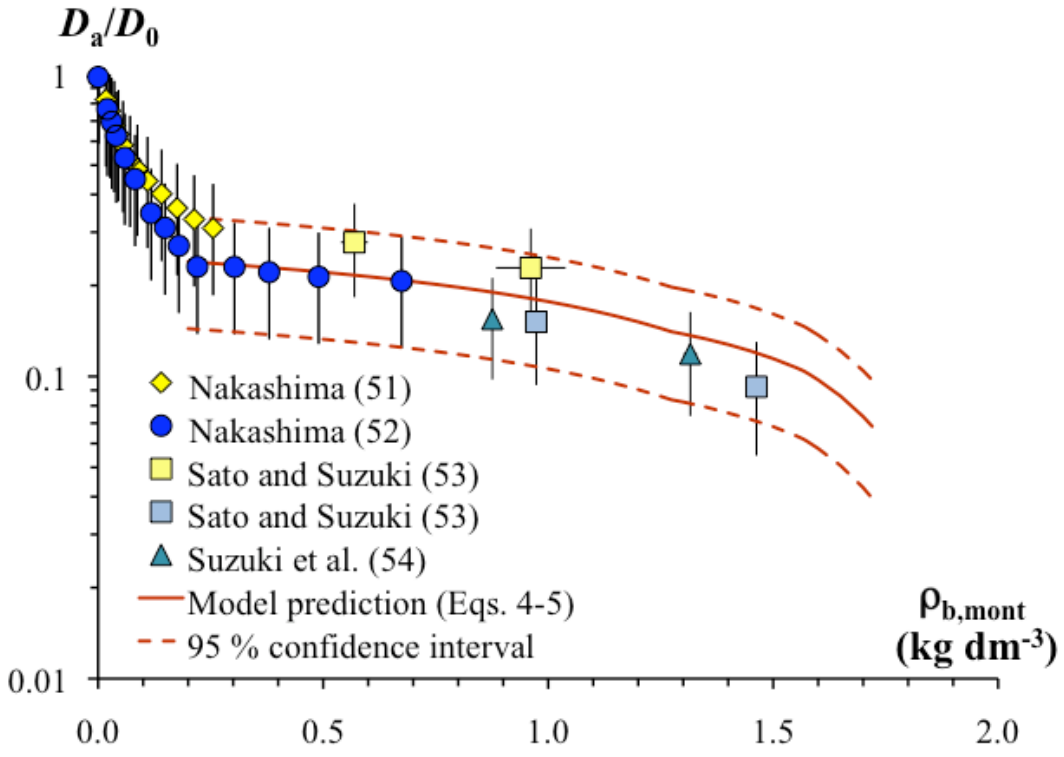
D_a/D_0
1
0.1
0.01
0.0
0.5
1.0
1.5
2.0
Nakashima (51)
Nakashima (52)
Sato and Suzuki (53)
Sato and Suzuki (53)
Suzuki et al. (54)
Model prediction (Eqs. 4-5)
95 % confidence interval
$\rho_{b,mont}$
(kg dm^{-3})

Figure 5.

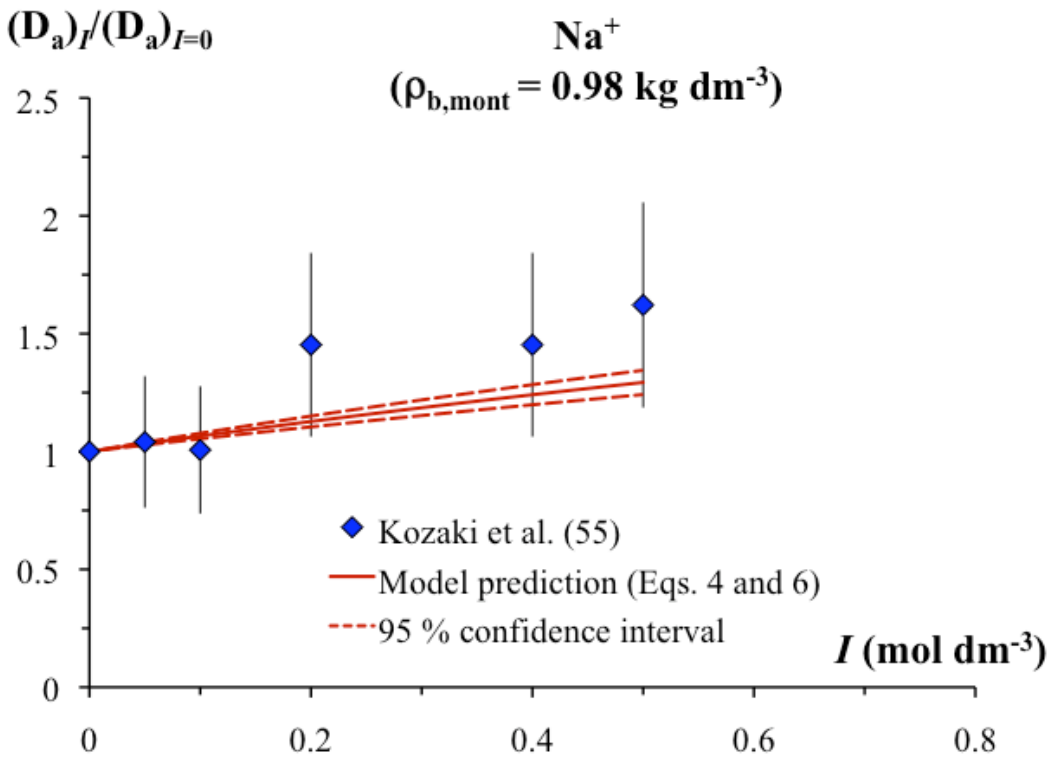
$(D_a)_I/(D_a)_{I=0}$
Na^+
($\rho_{b,mont}$ = 0.98 kg dm^{-3})
2.5
2
1.5
1
0.5
0
0
0.2
0.4
0.6
0.8
Kozaki et al. (55)
Model prediction (Eqs. 4 and 6)
95 % confidence interval
I (mol dm^{-3})

Figure 6.

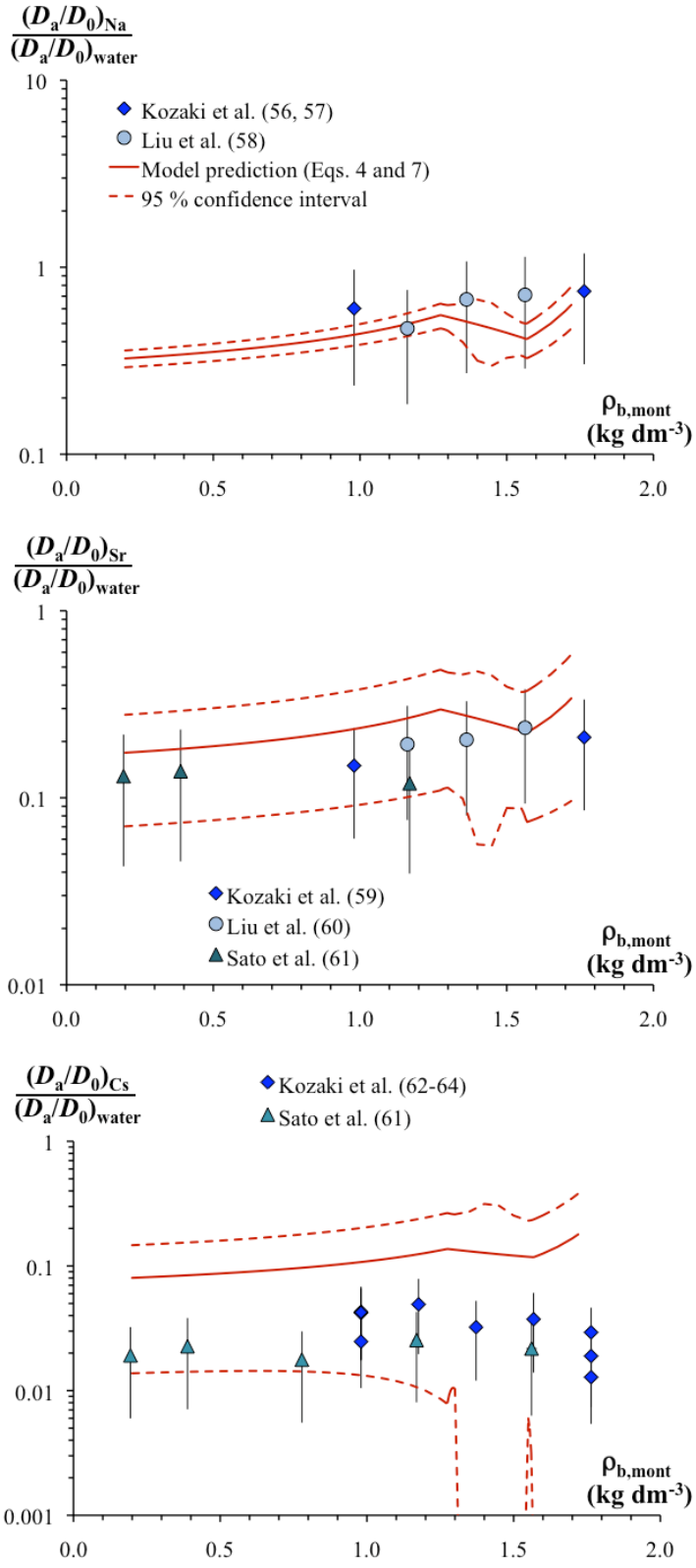
$(D_a/D_0)_{Na}$ / $(D_a/D_0)_{water}$
10
1
0.1
Kozaki et al. (56, 57)
Liu et al. (58)
Model prediction (Eqs. 4 and 7)
95 % confidence interval
$\rho_{b,mont}$ (kg dm^{-3})
0.0
0.5
1.0
1.5
2.0
$(D_a/D_0)_{Sr}$ / $(D_a/D_0)_{water}$
1
0.1
0.01
Kozaki et al. (59)
Liu et al. (60)
Sato et al. (61)
$\rho_{b,mont}$ (kg dm^{-3})
$(D_a/D_0)_{Cs}$ / $(D_a/D_0)_{water}$
Kozaki et al. (62-64)
Sato et al. (61)
1
0.1
0.01
0.001
$\rho_{b,mont}$ (kg dm^{-3})

Brief—A scaling expression for water and cation diffusion in clay barriers is consistent with molecular dynamics simulations of diffusion in smectite interlayer nanopores.